Modeling and Design of a five Degrees-of-Freedom Delta-Like Robot for Fast Pick-and-Place Applications

Valentin Le Mesle, Vincent Bégoc, Sébastien Briot

Modeling and Design of a five Degrees-of-Freedom Delta-Like Robot for Fast Pick-and-Place Applications

Valentin Le Mesle
MG-Tech Angers
École Centrale de Nantes
Laboratoire des Sciences du Numérique de Nantes (LS2N)
UMR CNRS 6004
44321 Nantes, France
Email: Valentin.Lemesle@ls2n.fr

Vincent Bégoc*
Institut Catholique d'Arts et Métiers (ICAM)
Laboratoire des Sciences du Numérique de Nantes (LS2N)
UMR CNRS 6004
44321 Nantes, France
Email: Vincent.Begoc@icam.fr

Sébastien Briot
Centre National de la Recherche Scientifique (CNRS)
Laboratoire des Sciences du Numérique de Nantes (LS2N)
UMR CNRS 6004
44321 Nantes, France
Email: Sebastien.Briot@ls2n.fr

Delta-like architectures are widely used for fast pick-and-place applications. When rotational degrees of freedom are required to perform a task, one or more UPU kinematic chains are usually added to transmit the torques from motors located on the base to the platform, in order to actuate a wrist. Packaging applications usually require five degrees of freedom, and two UPU chains are then used to actuate two rotational degrees-of-freedom (DOFs) on the end-effector. However, the UPU chain induces significant limitations for industrial use: it significantly constrains the workspace along the vertical direction and implies a backlash in the universal joints degrading the accuracy of the robot.

In this paper, we investigate an alternative to the UPU kinematic chain for designing Delta-like robots with five DOFs. Indeed, the actuation of a two-DOFs wrist is performed through the use of a kinematic chain based on a succession of parallelograms associated with a Delta-like leg.

After a description of the kinematic models of the modified leg and an analysis of its singularities, a design optimization procedure is presented in order to define suitable geometric parameters for a given industrial application. Finally, a prototype is presented and its performances are evaluated.

*Address all correspondence related to ASME style format and figures to this author.

1 Introduction

1.1 State of the art

Pick-and-place (PnP) tasks consist in the translation and rotation of an object between two locations. Classically, industrial applications aim to pick an object from a conveyor and place it on a second conveyor (or in a box) with a desired orientation around a vertical axis. In the Industry, these motions can be performed by Delta robots [1] equipped with an additional UPU limb (U and P stand respectively for universal and prismatic joints) transmitting the rotation of an additional motor placed on the robot base to the mobile platform [2].

For packaging applications, five degrees-of-freedom (DOFs) are often required: the four degrees of freedom mentioned previously, plus an additional rotation around an horizontal axis. In the industry, the most common way to achieve these tasks is to use Delta robots with two UPU limbs [3]. These limbs allow the transmission of the rotation of motors fixed to the robot frame to some mechanism embedded in the platform, which converts the motor rotation into the desired end-effector orientation.

The use of UPU limbs induces important drawbacks, such as the limitation of the workspace along a vertical axis, an increasing backlash over time leading to the decrease of the positioning accuracy of the end-effector and, consequently, to an increase of maintenance costs. The current solutions addressing UPU chains limitations can be divided into four main categories. First, some manufacturers have

proposed improved designs of the UPU chain to increase the robot's workspace along the vertical direction. For example, the company Autonox connects a UPU chain to a ball screw driven by two motors [4]. It is also possible to replace the prismatic joint with a passive parallel structure [5], or by a pneumatic cylinder [6]: this last approach allows to facilitate the insertion of products in deep and narrow boxes. However, all these kinematic chains require the use of universal joints and are therefore subject to a rapid increase of backlash over time.

A second category of solutions consists in replacing the UPU chain by another transmission mechanism. For instance, rotational mobilities can be provided to the end-effector by adding one or more motors, located on the platform [6], inside the distal parallelograms [7] or at the end of the proximal arm [8]. This allows to obtain up to six degrees of freedom but induces an important increase of the embedded mass, which degrades the dynamic performances. Kim [9] designed a Delta robot that contains a cable loop inside a Delta leg. This cable connects an embedded pulley on the platform to a winch fixed on the base and allows unlimited rotation. However, the embedded pulley occupies a large part of the platform, which limits the addition of extra degrees of freedom. In addition, the elasticity of cables can lead to a deterioration of the positioning accuracy of the end-effector.

The third category of solutions consists in using additional Delta legs to enable the transmission of rotational mobilities to a rigid [10, 11] or articulated [12, 13] platform. However, the obtained range of rotation of the mobility is limited. Thus, some designs use articulated platforms followed by a motion amplification mechanism. The work done on the H4 robot family [14] has led to the design of a variety of motion amplification mechanisms, using among others: a belt [15], a rack and pinion [16], or a cable-and-pulley system [17]. Other articulated platforms may use gears [18], ball screw actuation [19] or epicyclic gear [20]. Nevertheless, these designs only achieve rotation about a vertical axis and can hardly be extended to applications with five or more degrees of freedom.

Finally, additional rotational degrees of freedom can be obtained by modifying the architecture of the robot. For instance, the HEXA robot [21] and equivalent structures [22] provide six degrees of freedom from six identical legs. The three rotations provided to the platform are however limited, and cannot be exploited for pick and place applications. The Double Delta [23] robot is composed of two Delta robots: the first one allows the translation of a platform in space, and the second one allows the movement of a secondary platform, dedicated to the actuation of a wrist with three degrees of freedom. Although this solution provides the necessary mobilities for pick and place applications, the complexity of the wrist integrated into the platform induces a high production cost.

1.2 Contribution of this work

As discussed above, most of the research works dedicated to the design of Delta-like robots avoiding UPU limbs have been limited to the proposition of architectures with four DOFs. Very little work has been dedicated to the design of five or six-DOFs Delta-like robots with no UPU limbs even if, as mentioned earlier, these robots are very appealing for packaging applications.

These works aim to fill this gap, by proposing a Delta-like architecture with five DOFs which avoids the main drawbacks mentioned above, i.e.:

- Using UPU chains increases the internal backlash.
- Using embedded motors increases the weight of the moving masses and limit the dynamic performances.
- Using an articulated platform is suitable for four-DOFs applications, but can hardly be extended to five-DOFs (or more) packaging operations.
- The addition of extra legs limits the workspace size.

In this paper, we introduce a five-DOF Delta-like robot, composed of two modified Delta legs. To the best of our knowledge, this architecture has never been presented before. The proposed leg allows to transmit an additional rotation to the mobile platform through the use of a succession of parallelograms. This solution is lightweight and is expected to have high internal stiffness. As such, it can be seen as a viable solution for transmitting one to three rotational DOFs to the moving platform of a Delta robot. The aim of this paper is thus to analyze the kinematic performance of this new architecture, to present a method to optimize its geometric parameters in order to satisfy requirements fixed by an industrial partner, to introduce the design of a prototype and to analyze its performance. In particular, we would like to study the internal backlash appearing in the modified legs to evaluate its potential for replacing UPU limbs.

This paper is thus organized as follows: Section 2 provides a description of the modified leg. Section 3 is dedicated to the study of the geometrical and kinematic models of the five-DOF Delta-like robot, as well as an analysis of its singularities. Then, Section 4 presents an algorithm to optimize the geometrical parameters of the five-DOFs robot under study, based on industrial constraints and requirements. Finally, the last section is dedicated to the presentation of a pre-industrial prototype, as well as to experiments allowing to evaluate the working space of the robot, the minimal cycle time obtained for a reference trajectory, and the evolution of the internal clearances at the output of the modified leg.

2 Description of the architecture

The architecture studied in this paper, presented on Fig. 1, is composed of three limbs whose anchor points are equally spaced around the base. A mobile platform is connected to the limbs through six spherical (S) joints. Similarly to Delta-like architectures, this platform has three translational DOFs and remains horizontal. One of the limbs, noted *III*, is a classical Delta-robot limb made of one link actuated by a revolute (R) joint followed by a spatial parallelogram.

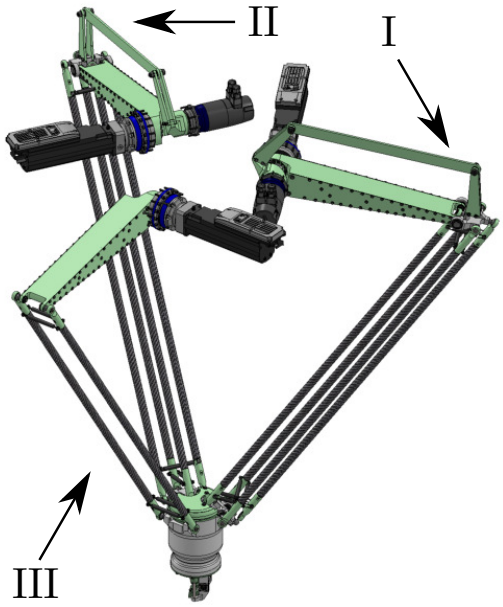

Fig. 1: CAD model of the proposed five-DOFs parallel robot.

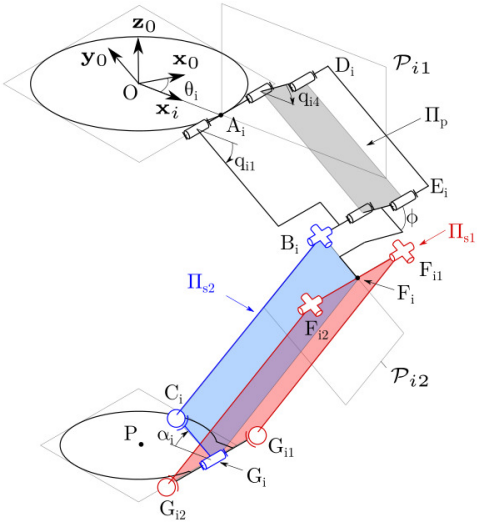

Fig. 2: Kinematic scheme of the modified limb. The proximal module lies in the plane $(O, \mathbf{x}_i, \mathbf{z}_0)$ denoted as $\mathcal{P}_{i1}$, and the distal module is expressed based on the plane $\mathcal{P}_{i2}$, which contains the parallelogram $B_iC_iG_iF_i$.

The two other limbs (noted *I* and *II*) connect the base to the mobile platform via a new kinematic chain detailed thereafter (Fig. 2).

This new limb is composed of two modules, a proximal module and a distal module (with respect to the robot's base). The proximal module consists of a planar parallelogram $A_iB_iE_iD_i$, later denoted as Π_p, which lies in the plane $(O, \mathbf{x}_i, \mathbf{z}_0)$ (named $\mathcal{P}_{i1}$ in Fig. 2). This module is actuated by two motors fixed to the robot's base. The first motor, $\mathcal{M}_{i1}$, actuates the link A_iB_i while the second motor $\mathcal{M}_{i2}$ actuates the link A_iD_i. The rotation of motor $\mathcal{M}_{i1}$ is denoted as q_{i1} (angle of the link A_iB_i with respect to the plane $(O, \mathbf{x}_0, \mathbf{y}_0)$) while the rotation of motor $\mathcal{M}_{i2}$ is denoted as q_{i4} (angle of the link A_iD_i with respect to the plane $(O, \mathbf{x}_0, \mathbf{y}_0)$).

The distal module is composed of two connected spatial parallelograms $F_{i1}F_{i2}G_{i2}G_{i1}$ and $F_iB_iC_iG_i$, later named Π_{s1} and Π_{s2} respectively. These parallelograms are presented on Fig. 3. The distal module is linked to the proximal module through the rigid link E_iF_i. As for a Delta robot, the spatial parallelogram Π_{s1} permits to constrain the horizontality of link $G_{i1}G_{i2}$ and, with the two other legs, constrain the horizontality of the platform. Indeed link $F_{i1}F_{i2}$ remains horizontal whatever the position of the two motors. A second spatial parallelogram Π_{s2} is introduced in order to provide a rotational motion of link C_iG_i with respect to the platform frame $(P, \mathbf{x}_0, \mathbf{y}_0, \mathbf{z}_0)$, by transmitting the rotation of link B_iF_i to link C_iG_i. The plane which which contains the spatial parallelogram $B_iC_iG_iF_i$ is named $\mathcal{P}_{i2}$. This parallelogram is composed of one universal (U) joint at B_i, one S joint at C_i and one R joint at G_i (whose axis is directed along $(G_{i1}G_{i2})$). In practice, U joints are obtained by constraining the S joints with springs, as it is commonly used for Delta-like robots. Further technological implementation details will be presented in Section 5.

By using two such modified limbs, two rotational DOFs

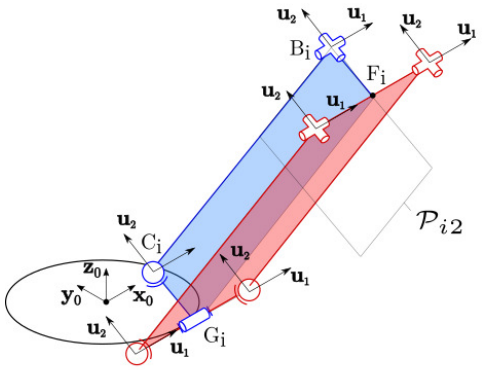

Fig. 3: Pair of parallelograms forming the distal module.

are then obtained on the platform, leading to a 5-DOFs architecture with two of them being rotations around non orthogonal horizontal axes. Note that by using such modified limbs, we may design robots from four to six DOFs, depending on the number of Delta limbs replaced by these new kinematic chain. Obviously, this architecture requires the use of a motion converter mechanism to convert the motion of links C_iG_i into the orientation and the tilt of an end-effector. An example of such mechanism will be presented in Section 5.

It should be emphasized that the actuation of links A_iB_i and A_iD_i leads to a coupled motion between the translations of the platform and the output angle α_i. More precisely, the actuation of A_iB_i leads to a pure translation of the platform, while the actuation of A_iD_i generates a translation of the platform and a rotation of link C_iG_i. It should be mentioned that this robot's architecture is currently being patented [24].

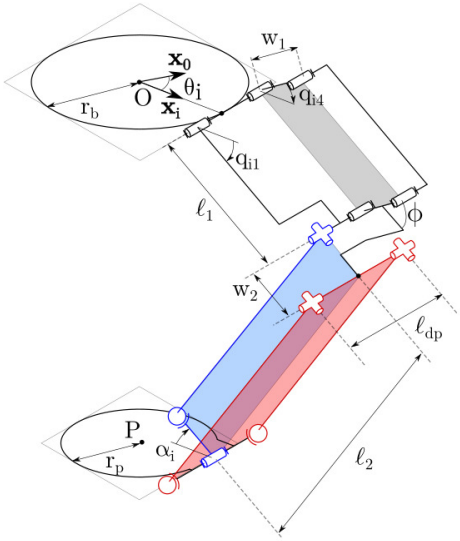

Fig. 4: Design parameters of the modified limb.

3 Geometry and kinematic models of the architecture

In what follows, the configuration of the platform of the proposed five-DOFs architecture is denoted as $\boldsymbol{\chi} = \begin{bmatrix}\mathbf{p}^T & \alpha_1 & \alpha_2\end{bmatrix}^T$, where $\mathbf{p} = \begin{bmatrix}x & y & z\end{bmatrix}^T$ corresponds to the location of point P (the center of the moving platform, and $\alpha_i = \angle C_i G_i P$ is the output angle of the corresponding modified limb.

The design parameters of the robot are displayed in Fig. 4. The base is modeled as a circle centered at O with a radius $r_b = \|\overrightarrow{OA_i}\|$, and the platform as a circle centered at P with a radius $r_p = \|\overrightarrow{PG_i}\|$. For both Delta and modified limbs, $\ell_1 = \|\overrightarrow{A_iB_i}\|$ and $\ell_2 = \|\overrightarrow{B_iC_i}\| = \|\overrightarrow{B_3G_3}\|$ (with $i = \{1,2\}$) correspond to the lengths of links A_iB_i and B_iC_i respectively, and $\ell_{dp} = \left\|\overrightarrow{F_{i1}F_{i2}}\right\|$ is the width of the spatial parallelogram Π_{s1}. The modified limbs include extra parameters: $w_1 = \|\overrightarrow{A_iD_i}\|$ is the length of the link actuated by $\mathcal{M}_{i1}$, $w_2 = \|\overrightarrow{B_iF_i}\|$ is the length of the link B_iF_i, which orientation depends on the actuation of both motors $\mathcal{M}_{i1}$ and $\mathcal{M}_{i2}$. Finally, $\phi = \angle E_iB_iF_i$ is the angular offset between the two parallelograms Π_p and Π_{s2}.

3.1 Inverse Geometric Model

Using the notations from Figure 4, the Cartesian coordinates $\mathbf{a}_i$ of point A_i in the base frame are expressed as:

$$\mathbf{a}_i = r_b\mathbf{e}_i \quad i = \{1,2,3\} \tag{1}$$

with $\mathbf{e}_i = \begin{bmatrix}\cos(\theta_i) & \sin(\theta_i) & 0\end{bmatrix}^T$, $\theta_i = \frac{2(i-1)\pi}{3}$ and $i = \{1,2,3\}$. The coordinates $\mathbf{b}_i$ of point B_i are equal to:

$$\mathbf{b}_i = \mathbf{a}_i + \ell_1\mathbf{m}_i \quad i = \{1,2,3\} \tag{2}$$

where $\mathbf{m_i} = \begin{bmatrix}\cos(\theta_i)\cos(q_{i1}) & \sin(\theta_i)\cos(q_{i1}) & -\sin(q_{i1})\end{bmatrix}^T$ is the orientation of the proximal link expressed in the base frame. In the actual design, two Delta legs corresponding to $i = \{1,2\}$ are modified. Given an end-effector pose $\boldsymbol{\chi} = \begin{bmatrix}\mathbf{p}^T & \alpha_1 & \alpha_2\end{bmatrix}^T$, $\mathbf{p} = \begin{bmatrix}x & y & z\end{bmatrix}^T$, the coordinates $\mathbf{g}_i$, $\mathbf{c}_i$ of points G_i and C_i are given by:

$$\begin{aligned}\mathbf{g}_i &= \mathbf{p} + r_p\mathbf{e}_i \quad i = \{1,2,3\}\\ \mathbf{c}_i &= \mathbf{g}_i + w_2\mathbf{n}_i \quad i = \{1,2\}\end{aligned} \tag{3}$$

with $\mathbf{n}_i = \begin{bmatrix}-\cos(\theta_i)\cos(\alpha_i) & -\sin(\theta_i)\cos(\alpha_i) & \sin(\alpha_i)\end{bmatrix}^T$. These expressions allow to write the following loop-closure equations:

$$\begin{aligned}h_i &= \mathbf{f}_i^T\mathbf{f}_i - \ell_2^2 = 0 \quad i = \{1,2\}\\ h_3 &= \mathbf{f}_3^T\mathbf{f}_3 - \ell_2^2 = 0\\ h_j &= \alpha_i - q_{i4} + \phi_i = 0 \quad i = \{1,2\} \quad j = \{4,5\}\end{aligned} \tag{4}$$

with $\mathbf{f}_i = \mathbf{c}_i - \mathbf{b}_i$ for $i = \{1,2\}$ and $\mathbf{f}_3 = \mathbf{g}_3 - \mathbf{b}_3$. From Eq. (4), the Inverse Geometric Problem of the robot can be solved as:

$$q_{i1} = 2\tan^{-1}\left(\frac{-I_i \pm \sqrt{I_i^2 + J_i^2 + K_i^2}}{K_i - J_i}\right) \tag{5}$$

with:

$$\begin{aligned}\text{For } i = 1,2: \quad & I_i = -2\ell_1(\mathbf{c}_i - \mathbf{a}_i)^T\mathbf{e}_i\\ & J_i = 2\ell_1(\mathbf{c}_i - \mathbf{a}_i)^T\mathbf{z}_0\\ & K_i = \|(\mathbf{c}_i - \mathbf{a}_i)\|^2 + \ell_1^2 - \ell_2^2 + w_2^2\\ \text{For } i = 3: \quad & I_i = -2\ell_1(\mathbf{g}_i - \mathbf{a}_i)^T\mathbf{e}_i\\ & J_i = 2\ell_1(\mathbf{g}_i - \mathbf{a}_i)^T\mathbf{z}_0\\ & K_i = \|(\mathbf{g}_i - \mathbf{a}_i)\|^2 + \ell_1^2 - l_2^2\end{aligned} \tag{6}$$

The additional actuation angle q_{i4} is obtained as follows:

$$q_{i4} = \alpha_i + \phi_i \quad i = \{1,2\} \tag{7}$$

3.2 Kinematic Model

The kinematic model can be obtained by differentiating Eq. (4) which, without detailing the calculations, leads to:

$$\mathbf{A}\dot{\boldsymbol{\chi}} + \mathbf{B}\dot{\mathbf{q}} = \mathbf{0} \tag{8}$$

with:

$$\mathbf{A} = \begin{bmatrix}\mathbf{f}_1^T & w_2\mathbf{f}_1^T\mathbf{s}_{\alpha_1} & 0\\ \mathbf{f}_2^T & 0 & w_2\mathbf{f}_2^T\mathbf{s}_{\alpha_2}\\ \mathbf{f}_3^T & 0 & 0\\ \mathbf{0}^T & 1 & 0\\ \mathbf{0}^T & 0 & 1\end{bmatrix};\ \dot{\boldsymbol{\chi}} = \begin{bmatrix}\dot{x}\\ \dot{y}\\ \dot{z}\\ \dot{\alpha}_1\\ \dot{\alpha}_2\end{bmatrix};$$
$$\mathbf{B} = \begin{bmatrix}\ell_1\mathbf{k}_1^T\mathbf{s}_{q_1} & 0 & 0 & 0 & 0\\ 0 & \ell_1\mathbf{k}_2^T\mathbf{s}_{q_2} & 0 & 0 & 0\\ 0 & 0 & \ell_1\mathbf{k}_3^T\mathbf{s}_{q_3} & 0 & 0\\ 0 & 0 & 0 & -1 & 0\\ 0 & 0 & 0 & 0 & -1\end{bmatrix};\ \dot{\mathbf{q}} = \begin{bmatrix}\dot{q}_{11}\\ \dot{q}_{21}\\ \dot{q}_{31}\\ \dot{q}_{14}\\ \dot{q}_{24}\end{bmatrix} \tag{9}$$

where $\mathbf{A}$ and $\mathbf{B}$ are respectively the forward and inverse Jacobian matrices, $\mathbf{k}_i = \mathbf{c}_i - \mathbf{a}_i$ for $i = \{1,2\}$ and $\mathbf{k}_3 = \mathbf{g}_3 - \mathbf{a}_3$, $\mathbf{s}_{\alpha_i} = \left[\sin\alpha_i \; 0 \; \cos\alpha_i\right]^T$, $\mathbf{s_{qi}} = \left[\sin q_i \; 0 \; \cos q_i\right]^T$. The Jacobian matrix $\mathbf{J}$ defined such that $\dot{\boldsymbol{\chi}} = \mathbf{J}\dot{\mathbf{q}}$ is then expressed as $\mathbf{J} = -\mathbf{A}^{-1}\mathbf{B}$ as long as $\mathbf{A}$ is not singular.

3.3 Singularity analysis

Serial or parallel singularities [25] appear when $|\mathbf{B}| = 0$ or $|\mathbf{A}| = 0$ respectively, where $|\mathbf{A}|$ and $|\mathbf{B}|$ denote the determinants for matrices $\mathbf{A}$ and $\mathbf{B}$. First, serial singularities appear if $\mathbf{f}_i$ and $\mathbf{s}_{qi}$ are orthogonal. In practice, this corresponds to the configurations where a) at least one leg is fully stretched or b), at least one vector $\mathbf{f}_i$ is orthogonal to its vertical leg plane $\mathcal{P}_{i1}$. Then, considering the shape of matrix $\mathbf{A}$, the determinant of $\mathbf{A}$ can be simplified as :

$$|\mathbf{A}| = |\mathbf{A}_\Delta| = \begin{vmatrix} \mathbf{f}_1^T \\ \mathbf{f}_2^T \\ \mathbf{f}_3^T \end{vmatrix} \tag{10}$$

where $\mathbf{A}_\Delta$ corresponds to the forward Jacobian matrix of the Delta robot. As a result, the parallel singularity conditions of the proposed robot and the Delta robot are similar [26, 27]. However, these matrices cannot be used to identify constraint singularities [28]. For this reason, the singularity analysis of the presented robot is performed hereafter using screw theory. Indeed, this geometric method aims to analyze the mobilities (twists) and the forces (wrenches) applied on the mechanism to extract singularity conditions. Here, this method is applied for a modified leg, and then, extended to the full robot.

The singular configurations of the proximal module of the modified leg (i.e. the parallelogram Π_p) are trivial and occur when the parallelogram is completely folded, leading to the condition $q_{i1} = q_{i4} + k\pi\,(k = 0, 1)$. Hence, screw theory is applied only on the distal module of the leg. Furthermore, q_{i1} and q_{i4} are considered to be fixed at constant values. To ease the study and without loss of generality, this study is carried on Π_{s1} and Π_{s2} separately.

First, considering the Delta parallelogram Π_{s1} (see also Fig. 3) symmetrical with respect to $\mathcal{P}_{i2}$, the set of twist screws $\$_\mathbf{t} = \{\$_{\mathbf{t}_{11}}, \$_{\mathbf{t}_{12}}, \$_{\mathbf{t}_{13}}, \$_{\mathbf{t}_{14}}\}$ of this kinematic chain is given by:

$$\begin{aligned} \$_{\mathbf{t}_{11}} &= (\mathbf{u}_{i1}, \mathbf{u}_{i1} \times \overrightarrow{OF_i}) \\ \$_{\mathbf{t}_{12}} &= (\mathbf{u}_{i2}, \mathbf{u}_{i2} \times \overrightarrow{OF_i}) \\ \$_{\mathbf{t}_{13}} &= (\mathbf{u}_{i1}, \mathbf{u}_{i1} \times \overrightarrow{OG_i}) \\ \$_{\mathbf{t}_{14}} &= (\mathbf{u}_{i2}, \mathbf{u}_{i2} \times \overrightarrow{OG_i}) \end{aligned} \tag{11}$$

with $\mathbf{u}_{i1}$ and $\mathbf{u}_{i2}$ the U joints axes. The wrench system $\$_\mathbf{w} = \{\$_{\mathbf{w}_{11}}, \$_{\mathbf{w}_{12}}\}$, which screws are reciprocal to the above twist system, is obtained by:

$$\begin{aligned} \$_{\mathbf{w}_{11}} &= (0, \mathbf{f}_i) \\ \$_{\mathbf{w}_{12}} &= (\mathbf{f}_i, \mathbf{f}_i \times \overrightarrow{OG_i}) \end{aligned} \tag{12}$$

Table 1: Design requirements for the desired application and minimal dimensions of a cylindrical Regular Dexterous Workspace (RDW).

Workspace diameter (m)	$d_{RDW} \geq d_{W0} = 1.2$
Workspace height (m)	$h_{RDW} \geq h_{W0} = 0.3$
Output angle range	$\alpha_{RDW} \geq \alpha_{W0} = 36^\circ$
LTI of the platform	$\mu \geq 0.3$
LTI of the parallelograms	$\sigma \geq \sin(30^\circ)$

The same procedure is applied on parallelogram Π_{s2}, giving the following set of twists and wrenches:

$$\begin{aligned} \$_{\mathbf{t}_{21}} &= (\mathbf{u}_{i1}, \mathbf{u}_{i1} \times \overrightarrow{OB_i}) \\ \$_{\mathbf{t}_{22}} &= (\mathbf{u}_{i2}, \mathbf{u}_{i2} \times \overrightarrow{OB_i}) \\ \$_{\mathbf{t}_{23}} &= (\mathbf{u}_{i1}, \mathbf{u}_{i1} \times \overrightarrow{OC_i}) \\ \$_{\mathbf{t}_{24}} &= (\mathbf{u}_{i2}, \mathbf{u}_{i2} \times \overrightarrow{OC_i}) \\ \$_{\mathbf{t}_{25}} &= (\mathbf{u}_{i1}, \mathbf{u}_{i1} \times \overrightarrow{OG_i}) \\ \$_{\mathbf{w}_{21}} &= (\mathbf{f}_i, \mathbf{f}_i \times \overrightarrow{OG_i}) \end{aligned} \tag{13}$$

The wrenches of the complete limb is obtained by the union of the two above wrench sets. The obtained wrench set is equal to $\$_\mathbf{w}$, and this result can be easily extended to the complete robot. As a result, the singularity conditions of the studied architecture are similar to a classical Delta robot [29], plus the conditions leading to at least one completely folded parallelogram, whether the planar parallelogram or one of the two spatial parallelograms.

The geometry and kinematic analyses carried in this section can be used to analyze the workspace of the proposed architecture. In the next section, an optimization problem is formulated to guarantee the accessibility of the end-effector to a prescribed cylindrical operation space satisfying minimal performance requirements.

4 Optimization Strategy

In this section, an optimization procedure used to obtain the optimal design parameters of the new architecture is presented.

4.1 Specifications

The requirements related to this work are presented in Tab. 1. These specifications have been imposed by the company MG-Tech, partner of the project. A cylindrical Regular Dexterous Workspace (RDW) [30] of diameter $d_{RDW} \geq 1.2$ m and height $h_{RDW} \geq 0.3$ m is desired. Furthermore, a minimal range of motion of the output angle α_i of each modified leg must be guaranteed throughout the cylinder, in order to actuate a motion converter mechanism. With our industrial partner, it has been considered that a range of motion

$\alpha_{RDW} \geq 36^\circ$ is sufficient for the input of the motion converter.

Then, a minimal motion/force transmission quality has to be guaranteed inside the cylindrical operational space. This performance is evaluated using the Local Transmission Index (LTI) [31] detailed later in this section. In this study, two LTIs have been used. A first LTI is related to the quality of transmission of the translational motion of the platform. This criterion can thus be used to compare the performances of the proposed robot with other Delta-like architectures. In this work, the minimum value of the LTI on the mobile platform is set to $\mu \geq 0.3$ throughout the operational space. A second LTI is related to the quality of transmission of the rotational motions, depending on the configuration of parallelograms Π_p and Π_{s2} (see Fig. 2). This index, also detailed later in this section, allows to find how far the parallelograms are from a singular configuration. In this work, the minimal value of the LTI on the parallelograms is set to $\sigma \geq \sin(30^\circ)$.

Finally, for practical industrial reasons (implementation of the robot inside a larger system), it is desired to design a robot as compact as possible. This objective, and the requirements mentioned previously and gathered in Tab. 1, are used to define an optimization problem detailed hereafter.

4.2 Design variables

The following assumptions are considered to reduce the number of design variables to optimize. First, the two modified limbs are identical. Thus, as presented in Fig. 4, the two modified limbs are described using the following parameters: ℓ_1, ℓ_2, w_1, w_2, ℓ_{dp} and ϕ. Moreover, it is decided that the lengths of the links A_iB_i, $F_{ij}G_{ij}$ and $F_{i1}F_{i2}$ of the Delta limb take the same values as those of the modified links, to ease the industrialization process. As a result, the geometric parameters describing the remaining Delta limb are ℓ_1, ℓ_2 and ℓ_{dp}.

Additional constraints on the geometry are imposed by the industrial partner: the radius of the platform is set to $r_p = 0.08$ m, the width of the planar parallelogram to $w_1 = 0.1$ m and the distance between points F_{i1} and F_{i2} to $\ell_{dp} = 0.117$ m. Thus, the input vector of this optimization problem is composed of the remaining design variables defining the radius of the base and the geometry of the limbs:

$$\mathbf{x} = [\, r_b \;\; \ell_1 \;\; \ell_2 \;\; w_2 \;\; \Phi \,] \tag{14}$$

4.3 Objective function

As mentioned previously, it is desired to minimize the footprint of the robot. Since the modified legs are identical, the compactness of the robot can be evaluated by computing the area covered by one modified leg, under the following configuration (see also Fig. 5):

- $\overrightarrow{OP}$ is vertical,
- points O, A_i, B_i and F_i are aligned,
- vector $\overrightarrow{OF_i}$ is horizontal,
- $\overrightarrow{OF_i}$ and $\overrightarrow{F_iG_i}$ are perpendicular.

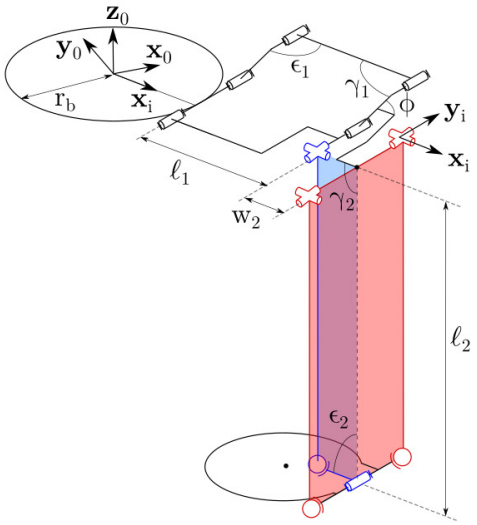

Fig. 5: Limb configuration for the computation of the objective function.

Thus, the objective function to be minimized is defined as:

$$\mathcal{A}_\ell = \ell_2(r_b + \ell_1 + w_2) \tag{15}$$

4.4 Constraints

In order to meet the requirements listed in Tab. 1, a set of four inequalities is introduced in the following. Two inequalities are related to the minimal LTI of the parallelograms and the platform respectively. Two other inequalities are introduced to make the realization of the prototype mechanically and practically feasible. These four inequalities must be satisfied among a Regular Dexterous Workspace (RDW). This RDW is a four-dimensional cylinder, the fourth dimension corresponding to the output angle α_i, with a diameter $d_{RDW} \geq 1.2$m, a height $h_{RDW} \geq 0.3$m and a range of rotation of the output angle $\alpha_{RDW} \geq 36^\circ$.

4.4.1 A minimal LTI for translational motions

The robot translational motion/force transmissibility is evaluated by computing a LTI based on the pressure angle $\delta_{i,j}$ [31,32] in the spherical joints connecting the distal links to the platform [33, 34] (Fig. 6). For each connection (i, j), the transmission index is expressed as:

$$\eta_{i,j} = \cos(\delta_{i,j}) = \frac{\mathbf{v}_{i,j}^T \hat{\mathbf{f}}_i}{\|\mathbf{v}_{i,j}\|} \tag{16}$$

where $\hat{\mathbf{f}}_i = [\frac{\mathbf{f}_i^T}{\|\mathbf{f}_i\|}, 0, 0, 0]^T$ describes the unit force (wrench) passing through F_iG_i, expressed at G_{ij}, and $\mathbf{v}_{i,j}$ is the displacement (twist) of the platform when only the link $F_{ij}G_{ij}$ is disconnected from the platform. This twist is expressed at the center of the spherical joint (i, j) located at G_{ij}. For a given spherical joint (i, j), this twist is computed as the kernel of a matrix, named $\mathbf{F}_{ij}$, which gathers the wrench screws

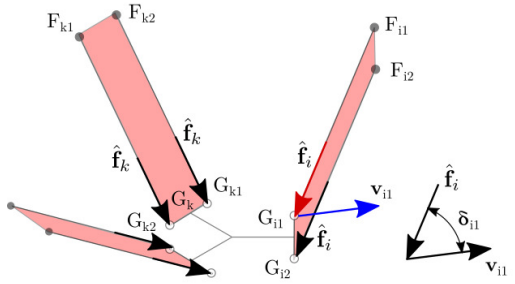

Fig. 6: Force and velocity vectors for the computation of the pressure angle δ_{ij}.

of the other spherical joints expressed at point G_{ij}. For instance, considering the spherical joint $(1,1)$ located at G_{11} and presented in Fig. 6, the corresponding matrix $\mathbf{F}_{11}$ is defined as:

$$\mathbf{F}_{11} = \begin{bmatrix} {}^{(1,1)}\$_{12}^T \\ {}^{(1,1)}\$_{21}^T \\ {}^{(1,1)}\$_{22}^T \\ {}^{(1,1)}\$_{31}^T \\ {}^{(1,1)}\$_{32}^T \end{bmatrix} \tag{17}$$

where:

$${}^{(i,j)}\$_{km} = \begin{bmatrix} \mathbf{f}_k \\ \overrightarrow{C_{km}C_{ij}} \times \mathbf{f}_k \end{bmatrix} \quad (i,j) \neq (k,m) \tag{18}$$

Finally, $\mathbf{v}_{i,j}$ is equal to:

$$\mathbf{v}_{i,j} = \ker(\mathbf{F}_{ij}) \tag{19}$$

This index and its minimal allowed value are then defined as in [35]:

$$\mu = \min\{\eta_{i,j}\} \geq \mu_{min} \quad \forall i = \{1,2,3\}, \forall j = \{1,2\} \tag{20}$$

The minimal LTI value allowed within the entire workspace is set to $\mu_{min} = 0.3$ as desired by our industrial partner.

4.4.2 A minimal LTI for rotational motions

This index [36] is used to evaluate how far the planar parallelogram $A_iB_iE_iD_i$ and the spatial parallelogram $B_iF_iG_iC_i$ are from a singular configuration. This index and its associated constraint are defined as:

$$\sigma = \sin\Big(\min\big(|\gamma_1|, |\gamma_2|, |\varepsilon_1|, |\varepsilon_2|\big)\Big) \geq \sin(30^\circ) \tag{21}$$

where $\gamma_1 = q_{i4} - q_{i1}$, $\gamma_2 = \angle BFC$ are the direct transmission angles and $\varepsilon_1 = \angle ADE$, $\varepsilon_2 = \angle FGC$ are the inverse

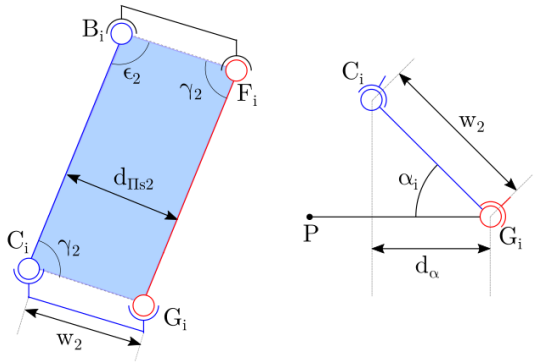

(a) Details on Π_{s2} projected in plane $\mathcal{P}_{i2}$ (b) Details on the platform projected in plane $\mathcal{P}_{i1}$

Fig. 7: Evaluation of the design constraints.

transmission angles of parallelograms Π_p and Π_{s2} respectively. These angles are presented on Fig. 5. The minimal acceptable value of this index within the workspace is set to $\sigma \geq \sin(30^\circ)$. For simplification purpose, Equation (21) is given for a single modified limb.

4.4.3 A minimal height for the distal parallelogram Π_{s2}

A minimal distance between $\overrightarrow{B_iC_i}$ and $\overrightarrow{F_iG_i}$ is desired to ease the assembly of a prototype. This distance, depicted in Fig. 7a is set to:

$$d_{\Pi_{s2}} = w_2 \sin(\gamma_2) > 0.03 \text{ m} \tag{22}$$

4.4.4 A maximal bulk of the platform

Finally, in order to ensure the modularity of the robot, the link C_iG_i needs to fit in the platform radius. Considering the design constraints related to the embedded motion converter mechanism, the final constraint is expressed as (see also Fig. 7b):

$$d_\alpha = \max(w_2 \cos(\alpha)) < 0.055 \text{ m} \tag{23}$$

where 0.055m is a threshold value provided by our industrial partner.

4.4.5 Minimal dimensions of the Largest Regular Dexterous Workspace

The aforementioned inequalities (20), (21), (22) and (23) have to be satisfied throughout the desired workspace of the robot. In order to simplify the formulation of the optimization problem, these four inequalities can be encapsulated into one general constraint related to the dimensions of the Largest Regular Dexterous Workspace (LRDW) such that:

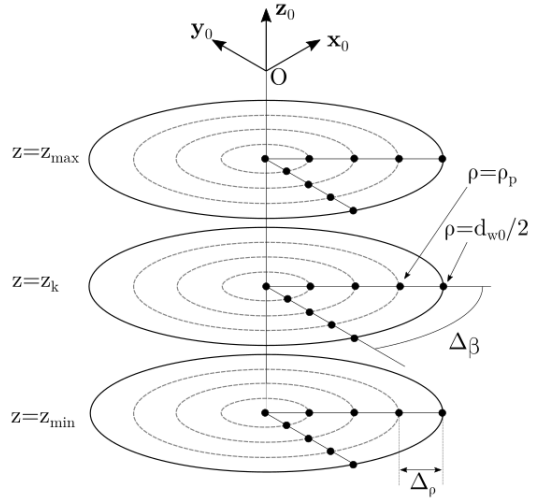

Fig. 8: Illustration of the discretization of the four dimensional cylindrical search space for a given output angle α_m.

$$d_{LRDW} \geq d_{W0} \tag{24}$$
$$h_{LRDW} \geq h_{W0} \tag{25}$$
$$\alpha_{LRDW} \geq \alpha_{W0} \tag{26}$$

where α_{LRDW} is the range of motion of the output angle α_i of the LRDW, d_{LRDW}, its diameter and h_{LRDW}, its height. The dimensions d_{W0}, h_{W0} and α_{W0} correspond to the industrial requirements specified in Tab. 1.

The method used to obtain the LRDW is detailed below.

4.5 Computation of the LRDW

This section presents an algorithm (detailed in Algo. 1) allowing to compute the LRDW of the robot. This algorithm is an adapted version of the algorithm detailed in [37]. First, a four-dimensional cylindrical search space is introduced (Fig 8) and discretized along the cylindrical coordinates (ρ, β, z) and the output angle α_i such that:

$$\begin{aligned} \rho \in \boldsymbol{\rho} &= [0 : \Delta_\rho : d_{W0}/2] \\ \beta \in \boldsymbol{\beta} &= [0 : \Delta_\beta : 2\pi] \\ z \in \mathbf{z} &= [z_{min} : \Delta_z : z_{max}] \\ \alpha_i \in \boldsymbol{\alpha} &= [\alpha_{min} : \Delta_\alpha : \alpha_{max}] \end{aligned}$$

with $\Delta_\rho = d_{W0}/(2N_d)$, $\Delta_\beta = 2\pi/N_d$, $\Delta_z = (z_{max} - z_{min})/N_0$ and $\Delta_\alpha = (\alpha_{max} - \alpha_{min})/N_0$, the steps' lengths, with $\alpha_{min} = 0$ and $\alpha_{max} = \pi/2$, and N_0 and N_d, the number of steps. z_{min} and z_{max} are user-defined parameters which define the minimal and maximal altitudes of the cylindrical search space. In the present application, these values are set to $z_{min} = -1.8$ m and $z_{max} = -0.3$ m.

The LRDW is obtained from a boolean matrix $\boldsymbol{\Omega}$, defined such that $\Omega_{k,m} = 1$ if all four inequalities (21), (20), (22) and (23) are satisfied among the whole discretized disk of height z_k for an output angle α_m, and $\Omega_{k,m} = 0$ otherwise:

Algorithm 1: Extraction of matrix $\boldsymbol{\Omega}$

```
Result: Ω
Initialized variables:
z = [z_min : (z_max − z_min)/N_0 : z_max];
α = [α_min : (α_max − α_min)/N_0 : α_max];
ρ = [0 : d_W0/2N_d : d_W0/2];
β = [0 : 2π/N_d : 2π];
Computation of the boolean matrix Ω:
for k = 1 : N_0 do
    for m = 1 : N_0 do
        for p = 1 : N_d do
            for q = 1 : N_d do
                Get σ, μ for [ρ_p β_q z_k α_m]^T;
                Get d_Π_s2, d_α for [ρ_p β_q z_k α_m]^T;
            end
        end
        if (20), (21), (22) and (23) ∀(p,q) ∈ [1,N_d]
          are satisfied then
            Ω_km = 1;
        else
            Ω_km = 0;
        end
    end
end
```

$$\Omega_{k,m} = \begin{cases} 1 \;\text{ if } \forall \rho \in \boldsymbol{\rho}, \forall \beta \in \boldsymbol{\beta}, z = z_k, \alpha = \alpha_m \\ \quad \text{and eq.(20), (21), (22) and (23) are satisfied} \\ 0 \text{ otherwise} \end{cases} \tag{27}$$

with z_k, the k-th element of the range $\boldsymbol{z}$ and α_m, the m-th element of the range $\boldsymbol{\alpha}$.

The location and size of the LRDW are then obtained by extracting the largest non-zero sub-matrix of $\boldsymbol{\Omega}$ using the algorithm detailed in [38]. The obtained sub-matrix is defined as a square matrix of dimension $(d \times d)$ and is identified by the indices (k_0, m_0) of its bottom right vertex. The height and angle range of the LRDW is thus expressed as:

$$\begin{aligned} h_{LRDW} &= \frac{d}{N_0}\Delta_z \\ \alpha_{LRDW} &= \frac{d}{N_0}\Delta_\alpha \end{aligned} \tag{28}$$

In the optimization process, these two parameters are evaluated in order to check that inequalities (25) and (26) are fulfilled. In the next section, the optimization problem is formulated and solved.

Table 2: Optimal solution chosen for a 5-DOFs robot

$\mathcal{A}_\ell$ (m^2)	ℓ_1 (m)	ℓ_2 (m)	r_b(m)	w_2(m)	ϕ(rad)
0.931	0.506	1.195	0.220	0.053	1.4975

Table 3: Location of the operational space obtained for the optimal solution ($h_{LRDW} = 0.3$ m and $\alpha_{min} = 36^\circ$)

z_{min} (m)	z_{max} (m)	α_{min} ($^\circ$)	α_{max} ($^\circ$)
-1.382	-1.082	12.4	48.4

4.6 Problem formulation and results

Based on the objective and constraint functions detailed above, the optimal design problem can be expressed as:

$$\begin{aligned} \text{Minimize} \quad & \mathcal{A}_\ell = \ell_2(r_b + \ell_1 + w_2) \\ \text{Over} \quad & \mathbf{x} = [\ \ell_1\ \ell_2\ r_b\ w_2\ \phi\ ] \\ \text{Subject to} \quad & h_{LRDW} \geq 0.3 \text{ m} \\ & \alpha_{LRDW} \geq 36^\circ \end{aligned} \tag{29}$$

This optimization problem has been solved by means of the MATLAB *fmincon* function using the 'active-set' algorithm, in order to deal with non-linear inequality constraints. The *multistart* algorithm from MATLAB has also been used in order to increase the chances to reach the global minimum. The optimal design parameters and its corresponding workspace are given in Tables 2 and 3. These values were used to design a prototype detailed in the next section.

5 Prototype and experiments

The following section aims to present and discuss the experimental results obtained on a proof-of-concept prototype. This prototype is a five-DOFs robot with two modified limbs and a two-DOFs wrist embedded on the moving platform. After a presentation of the prototype, the workspace of the robot is explored in order to validate the position and the size of the operational workspace predicted at the optimization stage. Then, the evolution of internal backlash in the modified limbs is evaluated and compared with that obtained with the UPU chain of the Delta robot currently manufactured by the industrial partner.

5.1 Description of the five-DOFs robot prototype and its two-DOFs wrist

In order to evaluate the performances of the proposed design, a prototype presented in Fig. 9 and Fig. 10 is assembled in MG-Tech's workshop. To facilitate the realization of the prototype, the parallelogram $B_iC_iG_iF_i$ is replaced by the parallelogram $B_{i1}C_{i1}C_{i2}B_{i2}$, as illustrated in Fig. 11. This small change of design has no impact on the kinematics of the mechanism and allows to use pretensionned springs

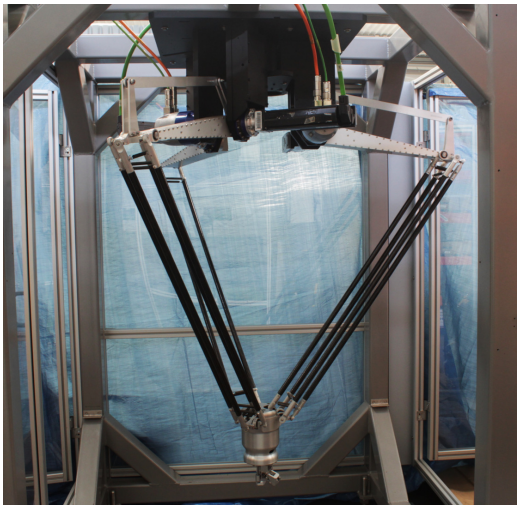

Fig. 9: Picture of a five-DOFs prototype realized and tested in the MG-Tech workshop. The robot uses two modified legs and the platform contains a motion converter allowing to obtain two independent rotations of the tool around a vertical axis $\mathbf{z}$ and a mobile horizontal axis $\mathbf{y}'$ directions.

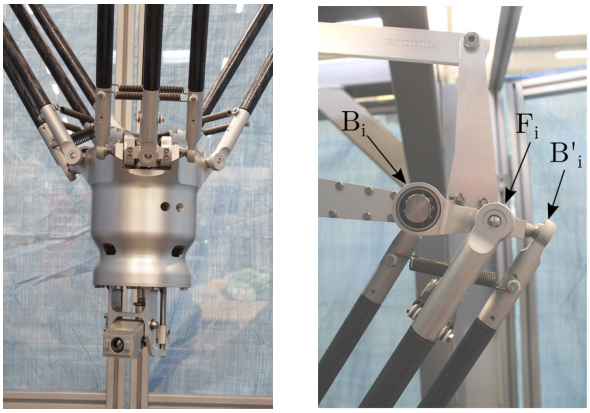

(a) Moving platform with the 2-DOFs wrist

(b) Top of the distal module

Fig. 10: Detailed view of the moving platform (left) and the connection between the proximal and distal modules (right). For the prototype, the parallelogram $B_iG_iC_iF_i$ is replaced by the parallelogram $B_iG_iG'_iB'_i$, which allows using spherical joints and pretensionned springs to obtain a spatial parallelogram

.

and spherical joints to realize the distal modules (Fig. 10). The angles q_{i1} are actuated by three motors with a maximal torque of 4.0 N.m connected to gear boxes with a ratio of 38.5. The two other angles q_{i4} and q_{i5} are actuated with motoreductors which can deliver a maximal torque of 100 N.m. These five motors are controlled with an industrial Schneider controller.

The platform of the robot's prototype contains a two-DOFs wrist (see a CAD view on Fig. 12) designed to obtain a rotation around axis $\mathbf{z}_0$ $\theta_z \in [-180^\circ, 180^\circ]$ from the rotation of angle α_1 and a rotation around an horizontal axis

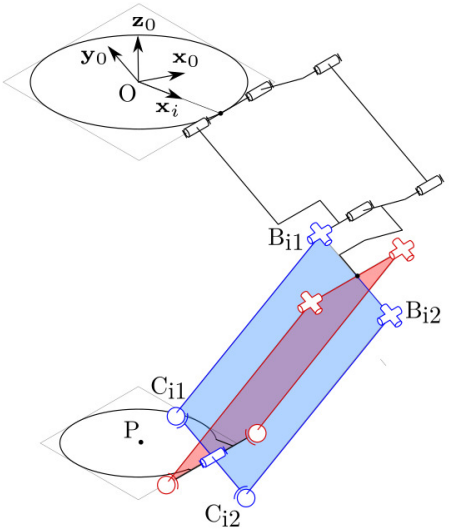

Fig. 11: Kinematic scheme of the modified limb used for the prototype. In this design, the link $B_{i2}C_{i2}$ is added to use pretensionned springs to hold the spatial parallelogram $B_{i1}C_{i1}C_{i2}B_{i2}$.

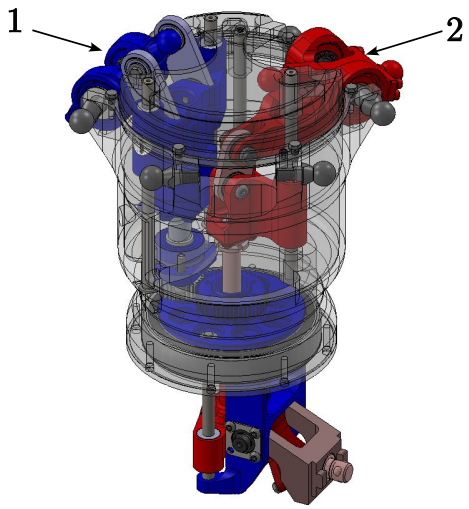

Fig. 12: CAD model of the two-DOFs wrist developed for the prototype. The wrist is composed of two sub-mechanisms. The first one, shown on the left and labeled as '1', allows converting the actuation of a modified limb into a 360° rotation around a vertical axis. The second sub-mechanism, shown on the right and labeled as '2', provides a 90° rotation around a moving horizontal axis.

$\mathbf{y}'$ $\theta_{y'} \in [0°, 90°]$ from the rotation of angle α_2. The wrist was designed so that rotations around $\mathbf{z}_0$ and $\mathbf{y}'$ can be actuated independently. This wrist is composed of two sub-mechanisms described below:

- The first sub-mechanism (shown on Fig. 13) provides a 360° rotation around axis $\mathbf{z}_0$. The output angle α_1 is used to translate a ball screw nut (1c) along a vertical axis. This translation of (1c) is converted into a rotation of the screw shaft (1d), which is attached to a former gear (1f) which causes the rotation of a second gear (1g) along axis $\mathbf{z}_0$. In the presented prototype, the screw has a pitch of 16 mm and its rotation is reduced by a gear ratio of 1.5. As a result, a 24 mm translation of the screw is required to obtain a 360° rotation of the end-effector around $\mathbf{z}_0$.
- The second sub-mechanism (shown on Fig. 14) is a crank rod which transmits a rotation α_2 around an horizontal axis to the end-effector. It has a magnification factor of 3, which allows a 90° range of rotation of the end-effector around the $\mathbf{y}'$ axis.
- In order to obtain independent rotations around $\mathbf{z}_0$ and $\mathbf{y}'$, the spur gear (2f) and the translating rod (1d) have coincident axes of rotation.

Since the design aims to ensure a lifespan of 80 million cycles, the components are designed accordingly leading to a bulkier design. As a result, the current platform (including the wrist) of the proof of concept prototype weights 5.5 kg. For future prototypes, a design optimization would help to minimize the weight of the wrist.

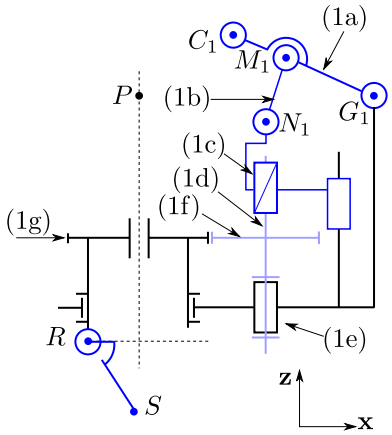

Fig. 13: The mechanism allowing to obtain a rotation of the end-effector around a vertical axis $\mathbf{z}$ from the output angle α_1. The actuation of the rod (1a) allows the translation of the nut (1c) through a connecting rod (1b). The rotation of the ball screw (1d), attached to a gear (1f), activates the rotation of gear (1g) on which the end-effector is fixed at point R. The end-effector is mounted on link RS.

5.2 Validation of the operational workspace

The first experiment aims to validate the workspace desired by our industrial partner, consisting of a cylinder of diameter $d = 1200$ mm and height $h = 300$ mm centered around axis $\mathbf{z}_0$. For this prototype, the cylinder is located between altitudes $z = -1082$ mm and $z = -1382$ mm. Using the symmetry of the architecture, the boundaries of the desired workspace are evaluated by verifying the accessibility of the platform for the extreme configurations of a modified leg. These extreme configurations are illustrated on Fig. 15. Then, a set of five-DOFs trajectories depicted in Fig. 16 have been used to explore the workspace. These trajectories draw dodecagrams on seven horizontal evenly spaced planes

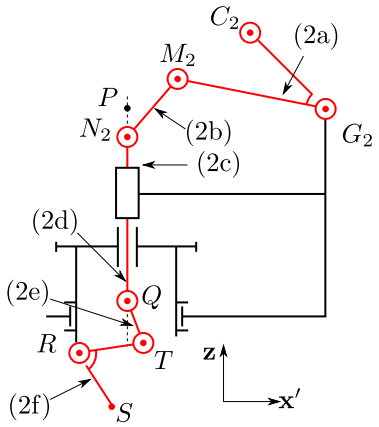

Fig. 14: A mechanism allowing to obtain a rotation of 90° around a mobile horizontal axis $\mathbf{y}'$ from the output angle α_2. The actuation of the link (2a) allows the translation of a rod (2d). The rotation of the end-effector is obtained by a tilting movement of link (2f) around point *R*. The end-effector is mounted on link *RS*.

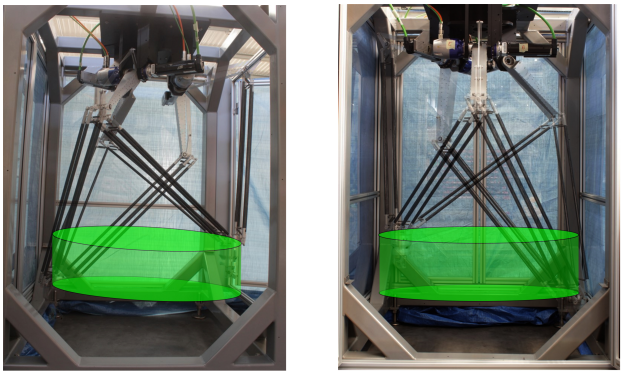

(a) First leg (b) Second leg

Fig. 15: Restricting configurations for the two modified legs. Using the symmetry of the architecture, these positions are used to verify the accessibility of the moving platform throughout the desired operational space, depicted in green.

within the desired workspace. The range of angular motion of the end-effector is verified by performing, for every segment of the dodecagram, a 360° rotation around a vertical axis $\mathbf{z}_0$ and a 90° rotation around a moving horizontal axis $\mathbf{y}'$. As a conclusion, the obtained results show that the robot is able to move in the prescribed workspace (Fig. 15).

5.3 Evaluation of the maximal production rate

In order to fit with industrial needs, it is desired to evaluate the minimal time needed to perform a typical pick-and-place application. This has been evaluated for a trajectory that is representative of a trajectory performed by robots on packaging lines installed by MG-Tech. This trajectory, presented in Fig. 17, corresponds to a classical pick-and-place trajectory between two conveyors spaced 700 mm apart, con-

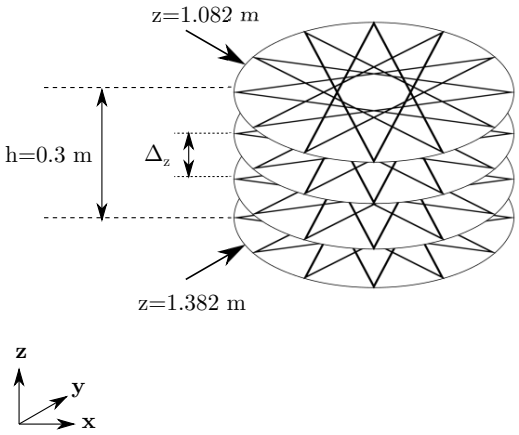

Fig. 16: Illustration of the trajectories used for the evaluation of the operational workspace of the prototype. The exploration is performed by drawing horizontal dodecagrams for different altitudes z spaced by $\Delta_z = 0.05$ m. For each segment, a rotation of the end-effector of 90° around a moving horizontal axis and a 360° rotation around $\mathbf{z}$ are performed. The orientation of the end-effector is returned to initial values $\theta_{y'} = 0$, $\theta_z = 0$ each time a vertex is reached.

sidering a tracking distance[1] of 200 mm and a vertical displacement of 300 mm. Rotational displacements of 90° along $\mathbf{y}'$ and 360° $\mathbf{z}_0$ are also imposed. In order to ensure a continuous acceleration profile, the trajectory is generated using a fifth-degree polynomial law motion. The linear and rotational velocities and accelerations of the trajectory were defined for each segments in such a way as to minimize the cycle time, without exceeding the I²T index for each motor [39]. This index is a manufacturer's threshold related to the thermal heating of a motor, which aims to improve its lifespan.

For the current prototype, the obtained production rate is 39 cycles per minute. It should be noted that better performances could be obtained using more appropriate actuators and a lighter wrist, but this is left to future works.

5.4 Evaluation of the internal backlash in a modified leg

This section details the measurement protocol and set up used to measure the rotational backlash obtained at the end of a modified leg. The aim is to evaluate the capacity of this leg to transmit rotational motions to a moving platform, in an accurate and durable manner. Due to the compact design of the wrist, measurements are performed indirectly at the end-effector and not directly on rods (1a) and (2a), meaning that we also measure the backlash induced by the transmission mechanisms of the wrist.

The rotational backlashes are measured after continuously performing classical pick-and-place trajectories (see Fig. 17), at a frequency of 39 cycles per minute. The backlash is measured at the end-effector for rotations around axes $\mathbf{y}'$ and $\mathbf{z}$, after a run-in period of 300k cycles and, repeatedly,

[1]The tracking distance refers to the displacement of a product along the conveyor's axis ($\mathbf{x}$) while the robot is moving from one conveyor to the other.

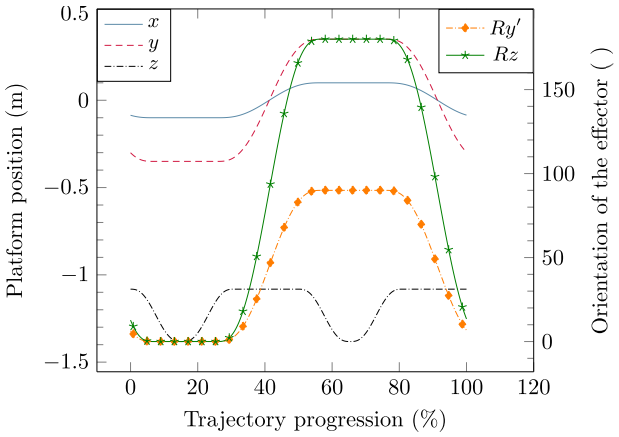

Fig. 17: Classical pick-and-place trajectory used to evaluate the minimal cycle time. The solid lines describe the translations of the platform, which follows a $200 \times 700 \times 300$ mm pick and place trajectory. The dashed lines represents the orientation of the end-effector, which covers 90° and ±180° rotations around $\mathbf{y}'$ and $\mathbf{z}$ respectively.

after 500k and 800k cycles (covering 1 % of the desired lifespan). The experimental setup, shown in Fig. 18, is composed of:

- a Mitutoyo dial gauge with a resolution of 0.01 mm, mounted on a fixed table measuring the horizontal displacement of a point located on the end-effector distant of 25 mm from the wrist $\mathbf{z}$ axis of rotation.
- a load connected to the end-effector through a pulley/cable system in order to apply a constant torque around the wrist $\mathbf{z}$ axis.

The process followed to measure the backlash at the end-effector for a rotation around the $\mathbf{z}$ axis is the following:

1. Apply a torque of respectively 1.2 N.m around the wrist's vertical axis.
2. Remove the torque and measure the remaining displacement with the dial gauge. The corresponding translational displacement is converted in an angular displacement noted δ_{θ^+}),
3. Repeat the two previous steps with an opposite torque. The corresponding translational displacement is converted in an angular displacement noted δ_{θ^-},
4. The total backlash is given as the sum of previous angular displacements : $\delta_{\theta_z} = \delta_{\theta^+} + \delta_{\theta^-}$
5. Repeat steps 1 to 4 five times.

A similar protocol was used to measure the backlash $\delta_{\theta_{y'}}$ around the moving axis $\mathbf{y}'$.

Values of the rotational backlash, in degrees, for the two axes $\mathbf{z}$ and $\mathbf{y}'$, are gathered in Tab. 4. After 800k cycles, results show an important backlash δ_{θ_z} at the end-effector (about 3.2°), whereas a negligible backlash $\delta_{\theta_{y'}}$ is obtained (about $1^\circ \times 10^{-4}$). Since the two modified legs actuating these two rotations were realized identically, it can be concluded that the important backlash δ_{θ_z} is mainly due to the

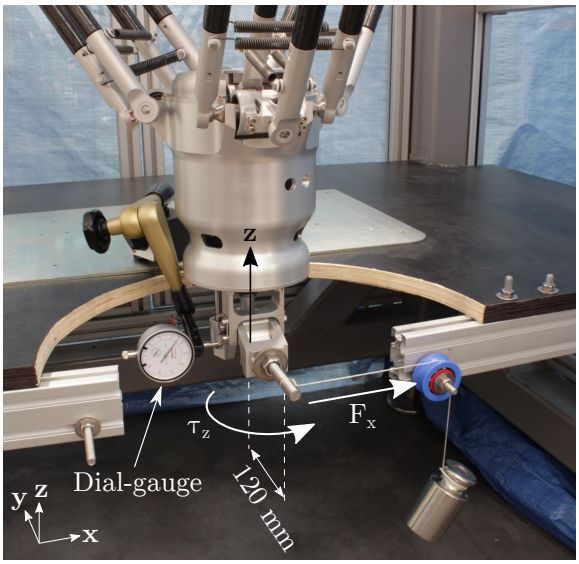

Fig. 18: Experimental setup used to measure the backlash at the end-effector around a vertical axis. A torque τ_z is applied on the end-effector by means of a mass connected to the end-effector via a cable/pulley system. The displacement of the end-effector is measured with a dial-gauge, which allows to compute the angular displacement.

Table 4: Measured backlash in degrees, obtained for the five-DOFs prototype, using modified legs for rotations.

	Number of cycles (kcycles)		
Angle (°)	300	500	800
$\delta_{\theta_{y'}}$	9.10^{-5}	9.10^{-5}	1.10^{-4}
δ_{θ_z}	3.1	2.9	3.2

Table 5: Measured backlash in degrees, obtained for MG-Tech's commercial Delta robot using UPU chains for rotations.

	Number of cycles (kcycles)		
Angle (°)	300	500	800
$\delta_{\theta_{y'}}$	$1.3.10^{-2}$	$1.4.10^{-2}$	$1.4.10^{-2}$
δ_{θ_z}	1.0	1.0	1.0

transmission mechanism included in the wrist, transmitting the rotation of the rod (1a) to the end-effector. Indeed, if the measured backlash came from the modified leg itself, $\delta_{\theta_{y'}}$ would have also been significantly high. A deeper investigation showed that the main source of the backlash δ_{θ_z} comes from the ball screw (1d) used to transform a translation of rod (1c) in a rotation around a vertical axis. Therefore, this means that the backlash measured at the end-effector is due to the two-DOFs wrist and does not come from the parallel-

ogram chains.

Obviously, the obtained results rely on many design parameters of both robots that are not detailed herein, however, this comparison between the prototype and the commercialized Delta robot is intended to evaluate the benefit of using a modified leg to transmit a rotational motion, with respect to a UPU chain.

For comparison purposes, a similar protocol was used to measure the backlashes obtained with a commercial Delta robot designed by MG-tech, equipped with two UPU chains. Results are presented in Tab. 5 and show that the backlash δ_{θ_z} is significantly higher for the prototype (3.2°) than for the commercial Delta robot (1°). On the other hand, the backlash $\delta\theta_{y'}$ is significantly smaller for the prototype (about $1^\circ \times 10^{-4}$) than for the commercial Delta robot (about $1.4^\circ \times 10^{-2}$). Obviously, the relevance of this comparison relies on many design parameters of both robots that are not all detailed herein, however, results show that the modified leg allows to obtain interesting performances with respect to a UPU chain.

As a conclusion, the realized proof-of-concept robot, using two modified legs, fits the company's expectations regarding the workspace size and the accuracy of the transmission of rotational degrees of freedom. Moreover, we may conclude that these modified Delta legs based on a succession of parallelograms are a viable alternative to UPU chains for designing Delta-like robots with additional rotations on the platform.

6 Conclusions

This paper introduces the design of a modified Delta leg which allows transmitting an additional rotational degree of freedom to the end-effector without the use of *UPU* chains. These rotations are provided by using a succession of parallelograms integrated on a Delta leg and driven by an additional motor attached to the base. Since the rotations provided by these legs are independent, it is possible to use up to three modified legs to obtain robots with up to six degrees of freedom.

After presenting the kinematics models and the singularity conditions of the proposed modified Delta leg, an optimization problem was introduced to obtain the geometrical parameters of a modified leg in order to minimize the footprint of a five-DOFs robot while guaranteeing minimal kinematostatic performances, based on the evaluation of the quality of the transmission of the forces on the mobile platform. These geometric parameters were then used to design a proof-of-concept five-DOFs prototype, consisting of a Delta structure incorporating two modified legs. A two-DOFs wrist was integrated on the platform to convert the rotations provided by the modified legs into a 360° rotation around a vertical axis and a 90° rotation around a moving horizontal axis.

A series of experiments were carried out on this prototype to validate the dimensions of the regular dexterous workspace desired by our industrial partner, as well as the minimum cycle time that could be obtained for a representative use-case. The rotational backlash at the modified leg output was measured indirectly, based on the values measured at the end-effector. Measurements realized after 800 000 cycles show a slight and steady increase of the backlash in the parallelograms and satisfy the requirements of our industrial partner. This, therefore, shows that the use of modified Delta legs with a parallelogram-based transmission mechanism is a suitable alternative to a UPU chain for transmitting a rotational degree of freedom for industrial pick-and-place operations.

Future works will focus on the industrialization of a five-DOFs Delta robot composed of two modified legs and on the improvement of the two-DOFs wrist embedded in the moving platform. These improvements will mainly concern the design of the wrist, in order to reduce the backlash obtained for a rotation around a vertical axis and minimize its weight.

Acknowledgements

The authors want to thank all the teams of our industrial partner MG-Tech, for their technical help, guidance and support throughout this project. We also thank Jean-Baptiste Izard (ALTED) for assistance in designing the 5-DOFs prototype.

References

[1] Clavel, R., 1990. Device for the movement and positioning of an element in space, US976582A.

[2] Ehrat, M., 2001. Robot pour manipuler des produits dans un espace à 3 dimensions, EP1129829A1.

[3] Wang, H., 2013. Spatial six-degree-of-freedom mechanism capable of separately controlling rotation motion and translation motion, CN102848375A.

[4] Ilch, H., 2018. Robot industriel, EP3352950A1.

[5] Zhao, X., and Wang, P., 2013. Telescopic space triple-translation parallel manipulator,CN103240729A.

[6] Mihara, N., and Sanada, T., 2014. Parallel robot, robot system, and assembly method for transfer system, US2014360306A1.

[7] Fujimoto, K., Kinoshita, S., Kurebayashi, H., Nagayama, T., Uemura, T., and Yamamoto, M., 2011. Parallel link robot, US2011097184A1.

[8] Monti, G., 2012. Dispositif pour déplacer et positionner un membre dans l'espace EP2517841A1.

[9] Kim, K. H., 2014. Parallel Link Robot Providing Additional Degree of Freedom by Wire Rope, KR101401463B1.

[10] Xie, F., and Liu, X.-J., 2015. "Design and Development of a High-Speed and High-Rotation Robot With Four Identical Arms and a Single Platform". *Journal of Mechanisms and Robotics,* **7**, p. 041015.

[11] Wu, G., Bai, S., and Hjørnet, P., 2016. "Architecture optimization of a parallel Schönflies-motion robot for pick-and-place applications in a predefined workspace". *Mechanism and Machine Theory,* **106**(C), pp. 148–165.

[12] Pierrot, F., and Company, O., 1999. "H4: a new family

of 4-DOF parallel robots". In 1999 IEEE/ASME International Conference on Advanced Intelligent Mechatronics (Cat. No.99TH8399), IEEE, pp. 508–513.

[13] Wu, G., 2018. SCARA parallel mechanism that moves with rectangle working space, CN207104907 (U).

[14] Pierrot, F., and Company, O., 1999. "H4: a new family of 4-dof parallel robots". In 1999 IEEE/ASME International Conference on Advanced Intelligent Mechatronics (Cat. No.99TH8399), pp. 508–513.

[15] Pierrot, F., Nabat, V., Company, O., Krut, S., and Poignet, P., 2009. "Optimal design of a 4-dof parallel manipulator: From academia to industry". *IEEE Transactions on Robotics,* **25**(2), April, pp. 213–224.

[16] Krut, S., Benoit, M., Ota, H., and Pierrot, F., 2003. "I4: A new parallel mechanism for scara motions". In 2003 IEEE International Conference on Robotics and Automation (Cat. No.03CH37422), Vol. 2, pp. 1875–1880 vol.2.

[17] Krut, S., Nabat, V., Company, O., and Pierrot, F., 2004. "A high-speed parallel robot for scara motions". In IEEE International Conference on Robotics and Automation, 2004. Proceedings. ICRA '04. 2004, Vol. 4, pp. 4109–4115 Vol.4.

[18] Pierrot, F., Marquet, F., Company, O., and Gil, T., 2001. "H4 parallel robot: modeling, design and preliminary experiments". In Proceedings 2001 ICRA. IEEE International Conference on Robotics and Automation (Cat. No.01CH37164), Vol. 4, pp. 3256–3261 vol.4.

[19] Krut, S., Company, O., Nabat, V., and Pierrot, F., 2006. "Heli4: A parallel robot for scara motions with a very compact traveling plate and a symmetrical design". In 2006 IEEE/RSJ International Conference on Intelligent Robots and Systems, pp. 1656–1661.

[20] Altuzarra, O., Şandru, B., Pinto, C., and Petuya, V., 2011. "A symmetric parallel Schönflies-motion manipulator for pick-and-place operations". *Robotica,* **29**(6), Oct., pp. 853–862.

[21] Pierrot, F., Dauchez, P., and Fournier, A., 1991. "HEXA: a fast six-DOF fully-parallel robot". In Fifth International Conference on Advanced Robotics 'Robots in Unstructured Environments, IEEE, pp. 1158–1163 vol.2.

[22] Hongo, K., 2016. Robot À tringles parallèles et structure À tringles parallèles.

[23] Wu, G., 2017. *Conceptual Design and Analysis of a 6-Axis Double Delta Robot Towards High Acceleration*, Vol. 408. Springer, 11, pp. 389–401.

[24] Briot, S., Bégoc, V., Le Mesle, V., Trebouvil, M., and Brisseau, P., 2022. Tool robot comprising at least one rotating arm.

[25] Gosselin, C., and Angeles, J., 1990. "Singularity analysis of closed-loop kinematic chains". *IEEE Transactions on Robotics and Automation,* **6**(3), June, pp. 281–290.

[26] Clavel, R., 1991. "Conception d'un robot parallèle rapide à 4 degrés de liberté". PhD thesis, EPFL. Place: Lausanne Publisher: EPFL.

[27] López, M., Castillo, E., García, G., and Bashir, A., 2006. "Delta robot: Inverse, direct, and intermediate Jacobians". *Proceedings of the Institution of Mechanical Engineers, Part C: Journal of Mechanical Engineering Science,* **220**(1), pp. 103–109. _eprint: https://doi.org/10.1243/095440606X78263.

[28] Zlatanov, D., Bonev, I. A., and Gosselin, C. M., 2002. "Constraint singularities of parallel mechanisms". In Proceedings 2002 IEEE International Conference on Robotics and Automation (Cat. No.02CH37292), Vol. 1, pp. 496–502 vol.1.

[29] Gregorio, R. D., 2004. "Determination of Singularities in Delta-Like Manipulators". *The International Journal of Robotics Research,* **23**(1), pp. 89–96. _eprint: https://doi.org/10.1177/0278364904039689.

[30] Merlet, J.-P., 2006. *Parallel robots*, 2nd ed ed. No. 74 in Solid mechanics and its applications. Kluwer Academic Publishers, Dordrecht ; Boston, MA.

[31] Sutherland, G., and Roth, B., 1973. "A Transmission Index for Spatial Mechanisms". *Journal of Engineering for Industry,* **95**(2), May, pp. 589–597.

[32] Takeda, Y., and Funabashi, H., 1995. "Motion Transmissibility of In-Parallel Actuated Manipulators". *JSME international journal. Ser. C, Dynamics, control, robotics, design and manufacturing,* **38**(4), pp. 749–755.

[33] Glazunov, V. A., Arkaelyan, V., Briot, S., and Rashoyan, G. V., 2012. "Speed and force criteria for the proximity to singularities of parallel structure manipulators". *J. Mach. Manuf. Reliab.,* **41**(3), May, pp. 194–199.

[34] Brinker, J., Corves, B., and Takeda, Y., 2018. "Kinematic performance evaluation of high-speed Delta parallel robots based on motion/force transmission indices". *Mechanism and Machine Theory,* **125**, July, pp. 111–125.

[35] Wang, J., Wu, C., and Liu, X.-J., 2010. "Performance evaluation of parallel manipulators: Motion/force transmissibility and its index". *Mechanism and Machine Theory,* **45**(10), Oct., pp. 1462–1476.

[36] Liu, X.-J., Li, J., and Zhou, Y., 2015. "Kinematic optimal design of a 2-degree-of-freedom 3-parallelogram planar parallel manipulator". *Mechanism and Machine Theory,* **87**, May, pp. 1–17.

[37] Germain, C., Caro, S., Briot, S., and Wenger, P., 2013. "Optimal Design of the IRSBot-2 Based on an Optimized Test Trajectory". In IDETC-CIE2013. V06AT07A056.

[38] Briot, S., Pashkevich, A., and Chablat, D., 2010. "Optimal technology-oriented design of parallel robots for high-speed machining applications". In 2010 IEEE International Conference on Robotics and Automation, IEEE, pp. 1155–1161.

[39] Schneider Electrics, 2022. Monitoring Load and Overload (I2T Monitoring). `https://product-help.schneider-electric.com/Machine\%20Expert/V1.1/en/Lx32sDr/Lx32sDr/Functions_for_Operation/Functions_for_Operation-23.htm` (Accessed: 2022-10-10).